ELONGATED CLOUD OF COLD ^{87}RB ATOMS: TOWARDS A BRIGHTER SOURCE OF NARROWBAND PHOTON PAIRS

ADRIAN NUGRAHA UTAMA

A thesis submitted in partial fulfillment of the requirements for the degree of Bachelor of Science with Honours

DEPARTMENT OF PHYSICS

NATIONAL UNIVERSITY OF SINGAPORE

2016

Once upon a time

In galaxy far far away

Somebody created a quantum computer

To calculate the answer to life the universe and everything

And the answer was simply 42

Acknowledgements

First and foremost, I would like to express my gratitude to my lab partner, Mathias Alexander Seidler for always supporting me in the experiments, for all the insightful physics / non-physics / anything discussions, and for being such a good physicist / engineer. Without his support and encouragement, I might probably still be stuck constructing the laser system.

Next, I would like to thank my supervisor, Prof. Christian Kurtsiefer for providing me the opportunity to work in his group and on this project. I thank him as well for the insightful discussions during the group meetings and lunches, and for being the most awesome PI ever.

Next in this 'gratitude' list is Victor Leong. He has taught, talked, and discussed with me a lot (about anything in general) since I joined this group. I would like to thank him as well for his endless support in the experimental side (and moral side) of things.

I would like to thank Ale Cere for the many discussions about Physics and scientific writing, Chi Huan for the insightful discussions on a lot of things, Janet for being my partner-in-crime, Matthias for his guidance during my first few weeks in the group, Brenda for her support in the construction side of the project, Wilson for our late-night discussions, Jianwei and Lijiong for being such nice office-mate to talk to, and all the other members in the group.

My special thanks number 1 go to the people who helped me proofread my thesis and made it sound infinitely better: Victor, Mathias, and Brenda.

My special thanks number 2 go to my classmates who made my Honours year very fulfilling: Bo Xue, Janet, Ray Chew, etc.

Last but not least, I would like thank my family and friends, for always supporting me and being there for me.

Summary

Narrowband photon pairs are a valuable resource to study the interaction between photons and atoms. They can be generated by four-wave mixing in a cloud of cold atoms exploiting a cascade decay scheme. One limitation of this technique is the trade-off between the pair production rate (brightness) and the bandwidth of the generated photons; in general, increasing the brightness also broadens the bandwidth due to the collective effects in the ensemble. We propose a scheme to address this issue by generating an elongated cloud of cold ^{87}Rb atoms and exploiting the asymmetry of the cloud.

We present the design and construction details of various ingredients necessary to produce the cold elongated cloud. To produce the required magnetic field, we performed numerical calculations to obtain suitable parameters for the racetrack coils, which we then built and tested. Next, we set up the laser system needed to implement the magneto-optical trap (MOT). Finally, we assembled the vacuum system and the necessary optics.

We successfully obtained an elongated cloud of cold ^{87}Rb atoms. In the near future, we will characterise the optical density of the cloud and study the effect of the cloud geometry and optical density on the brightness and bandwidth of the generated photon pairs.

Contents

List of Figures

LIST OF FIGURES

Chapter 1

Introduction

In 1994, Peter Shor gave a seminal lecture on how quantum computers, if they ever exist, can simplify problems that are considered hard in classical computers [1]. Since then, researchers around the world have been attempting to realise quantum computers using different quantum systems, such as cavities [2], trapped ions [3], trapped neutral particles [4], nuclear spins [5], quantum dots [6], superconductors [7], and so on. A comprehensive review on the physical implementation of these systems can be found in [8]. Nevertheless, as they are hard to implement and control, these technologies may very well still be of the distant future. DiVincenzo outlined a few criteria that any quantum systems must possess to perform any useful quantum computation [9]. The search for an excellent quantum system is still ongoing, but in the process we gain lots of insights from quantum-related experiments, which also further our understanding of the ever puzzling quantum theory.

One particularly interesting aspect to study is the interaction between photons and atoms. While photons interact weakly with the environment, and thus serve as excellent transmitter of quantum information ('flying' qubits), atoms (or atomic systems in general) are well localised, which makes them good storage of quantum information ('node' qubits) [10]. Strong coupling between photons and atoms has been demonstrated with cavities [2], but it is challenging experimentally to scale up these systems as cavities are hard to maintain and control. In 2008, Tey et. al. demonstrated the feasibility

to achieve strong interaction of light and a trapped single atom without using any cavity [11]. This opened up new possibilities for an efficient photon-atom interaction, and since then people have been exploring this frontier, using parabolic mirrors [12] and focusing lenses [13]. To achieve strong atom-photon interaction, one require large spatial and temporal overlap between the modes of the photons and atoms [14].

We consider the case of the interaction between a single photon and a single atom. To obtain significant temporal overlap, the bandwidth of the single photon is required to match the bandwidth of the atomic transition (natural linewidth). One way to produce such single photons is by generating narrowband photon pairs via four wave mixing cascade decay scheme, with detection of one photon of the pair serving as the herald [10]. However, this technique suffers from the trade off between the generation rate of the photon pairs (brightness) and the bandwidth of the single photon. That is, due to collective effects in the ensemble, the bandwidth of the single photon is larger than that of the atomic transition, and to obtain a narrower single photon bandwidth, we have to sacrifice the pair generation rate.

We thus propose a scheme to address this issue by producing an elongated cloud of cold atoms and exploiting the asymmetry of the cloud to obtain a higher optical density (OD) in one axis. By performing four wave mixing in that axis, we hope to achieve a brighter source of photon pairs.

In this thesis, we first present an overview on the motivation behind producing an elongated cloud of cold atoms. We then proceed with the discussion about the design and construction of the various building blocks necessary to produce such cloud. We will conclude with a sight of the elongated cloud and the future direction of this project.

1.1 A Brief Summary of Previous Works

In this section, we present a brief summary about some of the previous works [15] [16] in our lab that motivates our choice to explore elongated geometry in the cloud of cold atoms.

1.1.1 Narrowband Photon Pairs

Photons pairs generated from parametric processes exhibit strong timing correlation [17], which is a very useful property that has been exploited in many quantum optics experiments [18] [19] [13]. There are many ways to generate photon pairs; the most well known method is by spontaneous parametric down conversion (SPDC) [20]. However, the bandwidth of these photons (∼THz) are orders of magnitude larger than the natural linewidth of neutral atoms (∼MHz), limiting the interaction between the photon and the atom.

One interesting approach to this issue is as follows: if we want to interact photons with atoms, why not generate the photons using the same species of atoms? This method has some advantages because the generated photons are already resonant to the atomic transitions, and they should also have comparable bandwidths to the atomic linewidth. Thus, within our group, we have successfully generated narrowband photon pairs via four-wave mixing (FWM) cascade decay scheme in a cloud of cold ^{87}Rb atoms [10]. These photon pairs have larger bandwidths compared to the natural linewidths. This is due to the collective effects in the ensemble and will be elaborated in Section 1.1.3. The FWM scheme is depicted in Figure 1.1.

One interesting point to note about this photon pair source is that it exhibits a very strong violation of the Cauchy-Schwarz inequality (R = 8.4×10^6 [10]) between two independent classical fields [21]. This implies that the signal and idler photons are strongly time correlated with very few accidental coincidences. This violation is much larger than in similar FWM experiment performed in ^{87}Rb gas cells [22] (R = 11600).

1.1.2 Heralded Single Photons

If we detect one photon of a photon pair, we know that the other photon is also present with a high probability due to the strong time correlations. This is the concept of heralding; the detection of a photon heralds the presence of another photon. Heralding enables us to give the heralded photon a 'time stamp', such that we know when the heralded photon interacts with the system of interest. There exists a time distribution

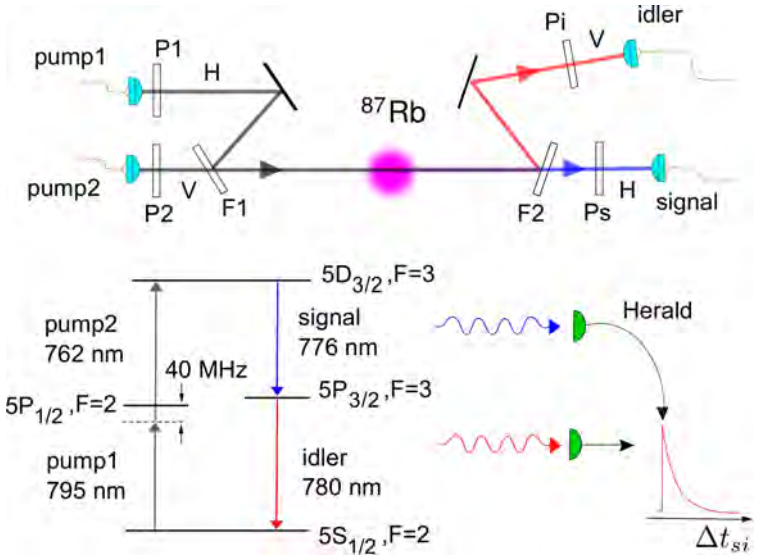

Figure 1.1: (Top) FWM scheme in cold ^{87}Rb atoms using collinear geometry. In this scheme, the pump beams of different polarisation direction are combined using an interference filter (F1). The generated signal and idler photons are then separated by another interference filter (F2), and the polarisers Pi and Ps select the polarisation of the photons. (Bottom) Cascade decay in ^{87}Rb atoms. When the signal photons are used as the herald, we obtain idler photons with exponentially decaying shape. Δt_{si} is the detection time of the idler photon heralded by the signal photon.

in the detection event of the heralded photons [17]. We can quantify this distribution using $g^{(2)}$ intensity correlation (known also as the temporal shape of the photon) [21].

The general scheme of photon heralding is depicted in Figure 1.1. We use the signal photon as the herald for the idler photon, which can then be sent to interact with the single atom. From the temporal shape of the idler photon, we can infer its coherence time. This coherence time is inversely related to the frequency bandwidth of the photon, as the photon has been shown to be Fourier-transform limited [10]. The idler photons are single photons (with n = 1 Fock state), as demonstrated in [23]. Interestingly, the temporal shape of the idler photon can be reversed by passing the signal photon to a cavity, obtaining idler photon with exponentially rising temporal shape [24]. This exponentially rising photon enables efficient excitation of the single atom, as this exci-

tation process would mimic the time-reversed process of the spontaneous decay of the single atom [14] [13].

1.1.3 Brightness And Bandwidth Trade Off

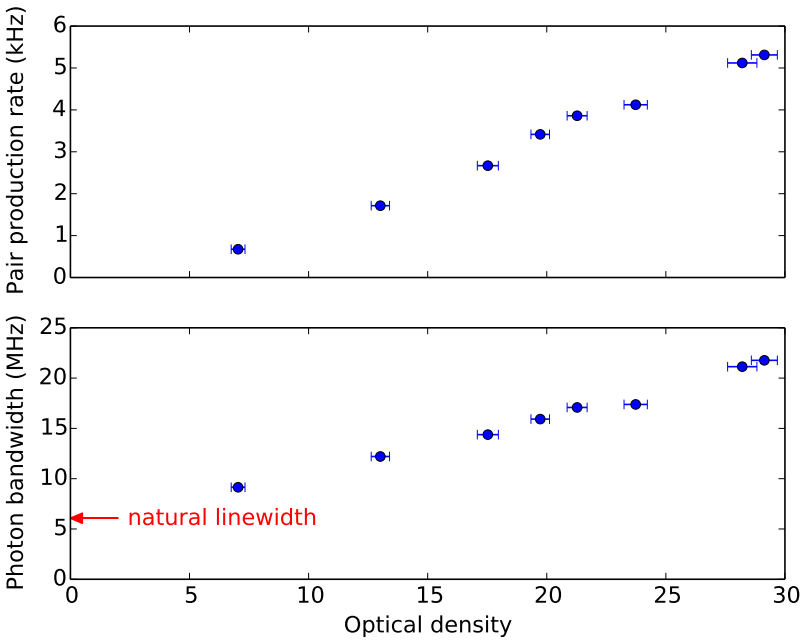

Figure 1.2: The effect of the OD of cold ^{87}Rb cloud on the photon pair production rate (top) and the bandwidth of the idler photon heralded by signal photon (bottom) [15]. The natural linewidth of the photon is 6.067 MHz, as depicted by the red arrow [25].

We can increase the optical density (OD) of the cloud by using a larger magnetic field gradient in the MOT to obtain a denser cloud with more atoms [15]. We have observed that the brightness and the bandwidth of the generated photons increase with a higher OD of the cloud (refer to Figure 1.2). However, it is not completely understood whether it is due to a cloud of higher OD having a larger total number of atoms or a higher atomic density.

The dependence of the bandwidth on the optical density is most probably due to superradiance: the effect of coherence in spontaneous radiation processes, which arises

if the atomic spacing is smaller than the photon wavelength [26] [27]. This effect has also been observed in similar FWM cascade decay experiments [19] [28].

To achieve efficient excitation of the single atom, we require bandwidth-matched photons, which can be achieved with low cloud OD. However, the brightness is painfully low in the low optical density regime. In our most recent experiment [13], the data acquisition took 6 months. Thus, there exists a trade off between the photon bandwidth and brightness.

1.2 The Proposed Scheme

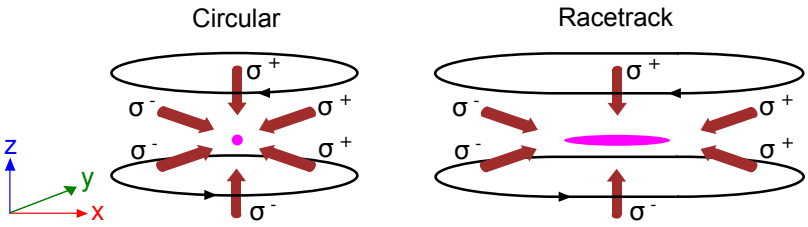

Figure 1.3: Two different expected shape of the cloud with different coil configurations. The coils produce magnetic field gradient necessary for the MOT. In addition, two pairs of horizontal laser beam and one pair of vertical laser beam provide radiation pressure to cool and trap the atoms inside the MOT. (Left) Circular anti-Helmholtz coils produce an almost spherical cloud. (Right) Racetrack anti-Helmholtz coils produce an elongated cloud.

We want to distinguish the effect of the optical density and atomic density on the brightness and bandwidth of the generated photons. Suppose the brightness depends strongly on the total number of the atoms (but not the atomic density) and the bandwidth depends strongly on the interatomic spacing (but not the total number of atoms). If that is the case, when we perform FWM in a long dilute cloud along the elongated axis, which has a large number of atoms (and hence OD) but low atomic density, we would have a bright source of photons with a bandwidth approaching the atomic linewidth.

The work in this thesis aims to test this hypothesis. We generate an elongated

cloud as depicted in Figure 1.3 (right). We cool and trap ^{87}Rb atoms in magneto-optical trap (MOT), which working principle is elaborated further in Appendix A. In order to achieve elongation, the magnetic field gradient in the elongation axis (x) has to be smaller than the other two axes (y and z), which can be obtained by using a pair of racetrack anti-Helmholtz coils.

Elongated clouds have been generated in a 2D-MOT [29] and 2D$^+$-MOT [30]. More recently, FWM has also been done in an elongated cloud [31], but a systematic study on how the cloud geometry affects the brightness and bandwidth of the generated photons has not been carried out.

Chapter 2

Design And Construction of An Elongated MOT

In this chapter, we present the details of the design and construction of the elongated MOT, in particular the magnetic field, laser system, and vacuum system. In order to achieve elongation in the cloud of cold atoms, there are two parameters that we can vary: the geometry of the magnetic field and the beam imbalance.

The size of the trap depends on the magnetic field gradient; the larger the magnetic field gradient, the smaller the trap size. Hence, in order to achieve elongation in one of the axes, the magnetic field gradient in that axis has to be lower than the other two axes.

We can also slightly alter the shape of the cloud by unbalancing the intensity of the laser beams. The laser beams are responsible for two tasks: creating a radiative pressure towards the centre of the trap and cooling the atoms. Thus, we can probably obtain slight elongation by having a lower laser intensity along one axis. However, this method is not as clear cut as the former method, as other factors might affect the elongation (the saturation of the laser transition, the collision between atoms in redistributing velocities, etc). We will possibly employ this method to perform some fine tuning on the cloud geometry if necessary.

2.1 Magnetic Field

We generate the necessary magnetic field gradient for elongation using a pair of racetrack shaped anti-Helmholtz coils. In this section, we discuss the details of the design, construction, and measurement of our racetrack coils.

2.1.1 Design

In designing the racetrack coils, we consider the following. Firstly, the coils should be big enough that we can fit a vacuum cuvette (3 cm $\times$ 3 cm $\times$ 10 cm) in between the coils, and preferably it should not be too big and bulky. Secondly, the magnetic field gradient in the elongation axis should be distinctively smaller (around 5 to 10 times) than the other two axes. Thirdly, the current of the coils should not be too high that it caused heating problem of the coils, while still be able to produce good enough magnetic field gradient (around 20 to 30 G/cm) for our experiments.

We perform numerical calculations to get an idea of the necessary dimension of the racetrack coils such that it satisfies the aforementioned considerations. The magnetic field is obtained by performing finite element numerical integrations of Biot-Savart Law using the SciPy package [32] in Python. After doing some calculations of the magnetic field, we chose the racetrack coils dimension as shown in Figure 2.1. Figure 2.2 shows a streamline plot of one cross section of the calculated magnetic field.

2.1.2 Construction

We proceed with constructing the racetrack coils using 18 American wire gauge (AWG) heavy polyimide enamel (HML) rectangular copper wire (the dimension of the wire cross section is 1.024 mm $\times$ 1.024 mm). We designed and 3D-printed plastic coil holders as the support for the coils. Next, we coiled and stacked the copper wire manually on the coil holder. A picture of the constructed racetrack coils is given Figure 2.3.

For our targeted magnetic field (around 20 - 30 G/cm on the y-axis or z-axis), the current of the coils is around 2 - 3 A. The total heat dissipation power of the coils (at

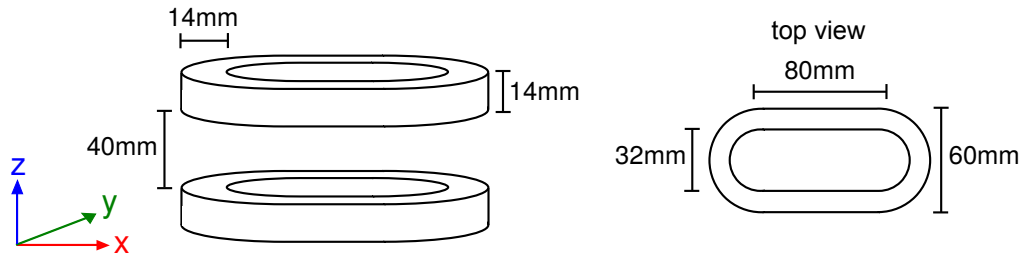

Figure 2.1: The dimension of our racetrack coils.

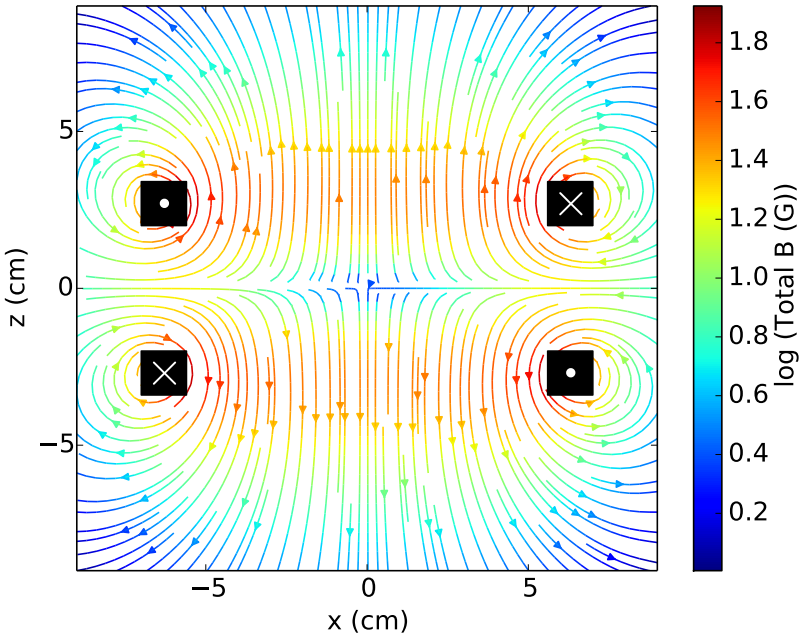

Figure 2.2: A streamline plot using Matplotlib [33] of the calculated magnetic field (at y = 0 plane). The origin of the plot is located at the centre of the trap. The current density of the coils is 1 A/mm^2, with the current direction shown with dots and crosses. The colour of the streamlines describe the magnitude of the magnetic field in base ten logarithmic scale.

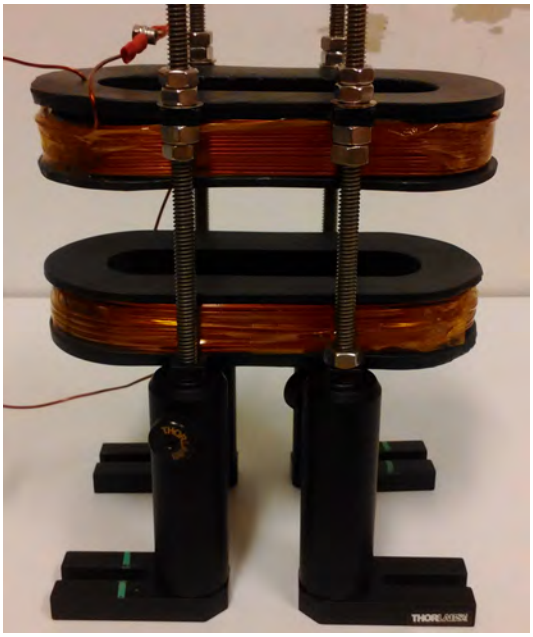

Figure 2.3: The picture of the constructed racetrack coils mounted on the holder.

2 A) is estimated to be around 8 W, and this should not create substantial heating problems and should not need additional cooling mechanisms. Moreover, the coil holder is made from plastic, and this should not create problems related with the Eddy current. As the entire process of construction (including 3D-printing and coiling) took us only 3 days, we can easily repeat the process and try out different coil dimensions, if necessary.

During the construction, we encountered some problems in the coiling process. Firstly, the 3D-printed plastic buckled slightly (examine Figure 2.3 carefully [1]), which meant the plastic material we used was not strong enough to withstand the stress during the coiling process. Secondly, as the holder slightly buckled, at some coiling layers we did not manage to fit the desired number of windings. We will look into these problems for the next iteration, but as these problems should not adversely affect our experiments, we moved on to the measurement.

[1] We can see that the holder slightly compresses in the centre (straight region) and slightly expands around the edges (circular region).

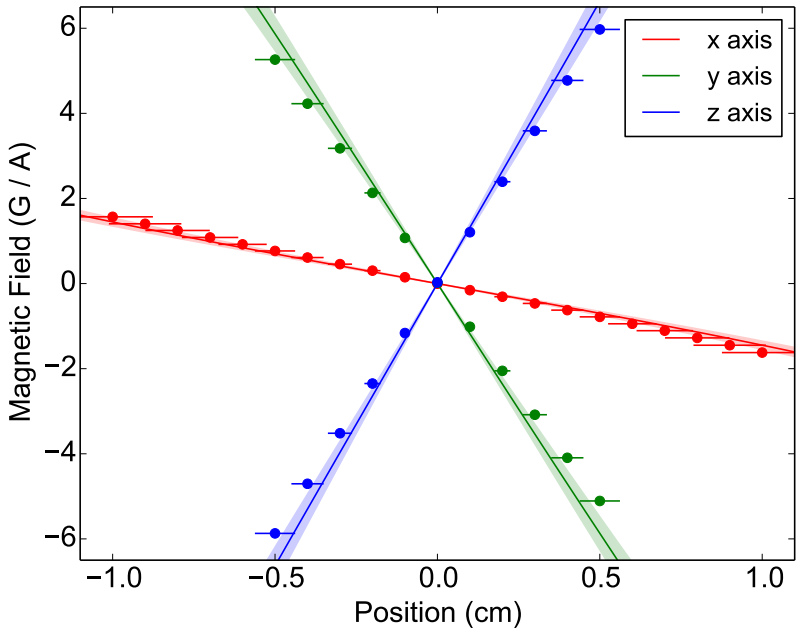

Figure 2.4: The comparison of the calculated magnetic field (solid lines) and the measured magnetic field (data points) of the racetrack coils in the three axes x, y, and z. The origin of the plot is located at the centre of the trap. The shaded area around theoretical line represents the estimated uncertainty in the expected value of magnetic field, which arises due to some construction problems as described in the previous section and the uncertainty in adjusting the distance between the coils. The vertical error bars (the uncertainty in the magnetic field measurement) are small and hence not shown in the figure, while the horizontal error bars are due to the estimated misalignment of the sensor.

2.1.3 Measurement

We measured the magnetic field created by the racetrack coils in the anti-Helmholtz configuration using a giant magnetoresistance (GMR) sensor (Honeywell HMC 1043). The comparison of the measured value with the numerically calculated value is given in Figure 2.4. From the data, we obtain a magnetic field gradient (MFG) of -1.6±0.2 G/A cm (in the x-axis), -10.4±1.3 G/A cm (in the y-axis), and -11.8±1.5 G/A cm (in the z-axis). The ratio of x-axis MFG to y-axis MFG is 0.15 ± 0.02, while the ratio of x-axis MFG to z-axis MFG is 0.13 ± 0.02.

2.2 Laser System

In this section, we first give a brief overview of the necessary components for building the laser system. Then, we discuss the targeted atomic transition and the laser system necessary to obtain the MOT.

2.2.1 Prerequisites

Basic Components

Here we give a brief desciption on some of the more basic optical components:

- Single mode optical fibre (SMF). SMF is an optical waveguide that only supports one spatial mode. It serves as an excellent resource to carry light from one location to another. We use aspheric lens to couple light into SMF and to collimate the light coming out from the fibre.

- Quarter Wave Plates (QWP). QWP is a birefringent material that modifies the polarisation of the incoming light by creating a retardation of $\lambda/4$ of between the o-axis and e-axis. Depending on the orientation of the QWP, we can create elliptically or circularly polarised light from linearly polarised light.

- Half Wave Plate (HWP). Similar to QWP, but with a retardation of $\lambda/2$ between the o-axis and e-axis. This enables HWP to rotate a linear polarisation to any other linear polarisation.

- Polarising Beam Splitter (PBS). PBS splits the incoming light into two directions depending on the polarisation. For the PBS that we use, the transmitted light is horizontally polarised, while the reflected light is vertically polarised. By using a HWP with a PBS, we can vary the splitting ratio of the light.

- Faraday Isolator (FI), also known as the optical isolator. FI only allows light to be transmitted in one direction by exploiting the Faraday effect. We used FI to prevent any undesired feedback to the lasers and the tapered amplifiers.

- Rubidium Gas Cell (Rb GC). Rb GC contains vapour of Rb atoms at room temperature. We use Rb GC in the laser spectroscopy as the source of Rb atoms.

External Cavity Diode Laser (ECDL)

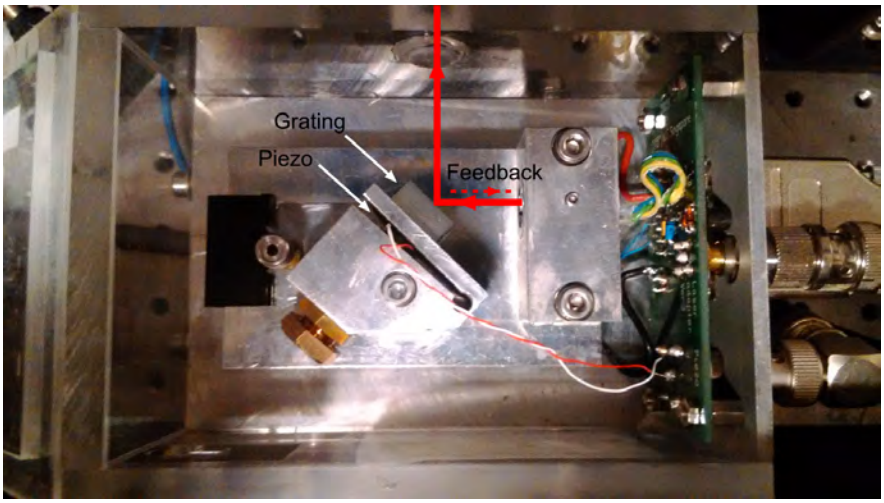

Figure 2.5: The picture of the ECDL in Littrow configuration.

ECDL is a laser module that produces narrowband ($\sim$ MHz) and frequency-tunable light out of a laser diode. Our ECDL utilised the Littrow configuration [34] as depicted in Figure 2.5. The laser beam is produced by a laser diode sitting inside a collimation tube, which collimates the outgoing laser beam with an aspheric lens. A diffraction grating reflects a small fraction of the light back to the laser diode as an optical feedback. The grating and the laser diode act as an 'external cavity', thus producing narrowband light out of ECDL.

ECDL frequency changes with the grating angle, temperature, and laser current. By varying these parameters, we can roughly tune the frequency to the desired frequency. Firstly, we adjust the grating angle to bring the ECDL frequency to around 100 GHz range from the targeted frequency. Then, by slightly varying the laser diode temperature and the laser current using a home-built laser driver, we can tune the ECDL frequency to within 1 GHz from the desired frequency.

To fine tune the ECDL frequeny, we supply different voltages to the piezo (material that responds linearly to the electric field by expanding or contracting) to adjust very slightly the length of external cavity. The sensitivity of the fine tuning with the piezo is around 0.5 GHz/V in our ECDLs. We use laser spectroscopy to lock and stabilise our laser to a specific atomic transition via the voltage feedback to the piezo. Refer to Appendix B for more detailed discussion on the spectroscopy techniques that we utilised.

Electro-Optical Modulator (EOM)

EOM is an optical component that modulates the frequency of a laser. The core of EOM is a crystal which index of refraction changes with the application of electric field, which is produced by the capacitor sandwiching the crystal. To drive the EOM, we apply a radio frequency (RF) to the capacitor, which creates oscillating index of refraction and thus modulating the incoming beam. In our experiments, the RF frequency is created by using a home-built direct digital synthesizer (DDS).

The effect of the modulation (in the frequency domain of the laser) is the creation of two sidebands at $\pm\Delta$ away from the laser frequency, with Δ as the modulation frequency. These sidebands are necessary in laser spectroscopy as described in Appendix B.

Acoustic-Optical Modulator (AOM)

AOM consists of a piezoelectric transducer that applies travelling RF acoustic waves to a crystal, creating a modulation in the crystal index of refraction. This creates effectively a diffraction grating, which splits the incoming light in a few diffraction orders. The AOM also increases or decreases the diffracted light frequency depending on the direction of the acoustic wave.

In our experiments, we use the AOM provided by Crystal Technology (3080-122 for 80 MHz AOM and 3080-124 for 200 MHz AOM). In the first diffraction order, the outgoing light frequency is $\omega \pm \Delta$, where ω is the incoming light frequency and Δ is

the modulation frequency. By adjusting the incident angle of the incoming beam, we can also optimise the amount of the light in certain diffraction order. The maximum diffraction efficiency of AOM is around 90 percent (with proper focusing of the incoming beam).

In our experiments, there are two purposes for using AOM. Firstly, the AOM allows us to tune the light frequency by around tens or hundreds of MHz. Secondly, it can act as a light switch, i.e. there will be no diffraction if no RF is supplied to the AOM.

There are two ways to incorporate AOM into the system: single pass and double pass. In a single pass setup, the light is passed through the AOM once with the outgoing beam angle changing with different modulation frequencies, making coupling to the fibre a tricky business. In a double pass setup, however, the diffracted light from the AOM is retro-reflected back to the AOM, passing the AOM twice. Therefore, the outgoing beam travels along the same path as the incident beam. By using combinations of HWP, QWP, and PBS, we can extract out the outgoing beam from the path. Thus, in double pass, we do not have a problem of coupling the outgoing beam into the fibre, but the overall efficiency is lower than for the single pass configuration.

2.2.2 Implementation

As outlined in Appendix A, we require a cooling laser red detuned from a cycling transition for the MOT. The cycling transition is chosen such that the cooling and trapping process can repeat many times without undergoing transition to any dark levels. In our case, we choose ^{87}Rb cycling transition from $5^2S_{1/2}$ (F = 2) to $5^2P_{3/2}$ (F' = 3), with a small red detuning in the order of tens MHz.

There is still a small probability for the F = 2 to F' = 2 transition to happen, which might bring the atom to the F = 1 dark state. Thus, we need another repump laser (tuned to the F = 1 to F' = 2 transition) to bring back atom to the cycling process. The ^{87}Rb energy level with the targeted atomic transitions is shown in Figure 2.6. The required wavelength for both the cooling and repump lasers are 780 nm [25].

The laser system is the workhorse of the experiment, and it took most of our space-

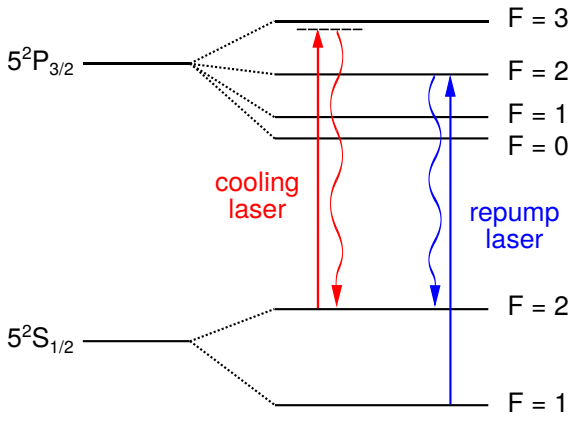

Figure 2.6: The hyperfine energy level of ^{87}Rb D_2 line, with the targeted cooling and repump transitions.

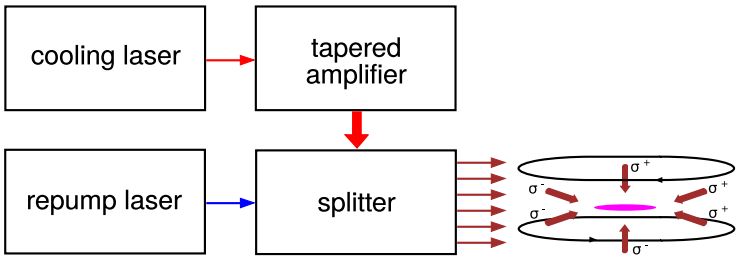

Figure 2.7: The overview of the laser systems. Each box represents separate modules, which are interconnected by using optical fibres. This modular system enables independent testing and debugging.

time [1]. We started with an empty optical table, and proceeded with building, testing, and debugging each laser system module. The overview of the laser systems is depicted in Figure 2.7.

The cooling and repump laser modules contain mostly components for laser stabilisation. As the MOT requires high cooling light power (around 20 mW for each beam), we amplify the cooling laser with the tapered amplifier (TA) module. The amplified cooling laser and the repump laser are combined and then split (in the splitter module) into the six MOT beams.

[1] This is meant to be a pun: the laser system took up most of the space on the optical table, while the construction process consumed most of our time.

Cooling Laser Module

Figure 2.8 depicts the schematic of the cooling laser module. The light from ECDL is split into two parts. Most of the light (around 15 mW) is coupled to a fibre and sent to the tapered amplifier, while a smaller portion (around 2 mW) is used for modulation transfer spectroscopy (MTS) to stabilize and lock the laser to the cooling transition. Refer to Appendix B for a more detailed overview on MTS.

The cooling light needs to be slightly red-detuning (tens of MHz) from the cycling transition, and we also require the capability to switch the cooling light on and off during the four-wave mixing pair generation process. To achieve this, we place a 200 MHz AOM (single pass) before the MTS and another 200 MHz AOM (single pass) after the tapered amplifier. Two AOM combined provides a way to obtain a small red detuning of the laser, i.e. one of the AOM shifts the laser frequency up, while the other shifts the laser frequency down. We use the former AOM to vary the red-detuning of the cooling light, while the latter AOM acts as the light switch.

Repump Laser Module

The schematic of repump laser module is given in Figure 2.9. The repump laser module is similar to the cooling laser module. However, as the sole purpose of repump laser is to bring the atoms in $F = 1$ state back to the cycling transition, we do not require high optical power, and thus we do not need a TA. The repump light is tuned on resonance to the specified transition, and we do not particularly need to switch the repump light on and off. Hence, we do not need to use any AOMs. The frequency lock uses the frequency modulation spectroscopy (FMS) technique (see Appendix B).

Tapered Amplifier Module

Tapered amplifier (TA) is an optical gain medium with tapered waveguide that amplifies the incoming laser. We used a TA chip from Eagleyard (EYP-TPA-0780-02000-3006-CMT03-0000) with a maximum laser output power of 2W. We drive the TA chip using a Thorlabs laser driver current controller (LDC240C) and stabilise the temperature

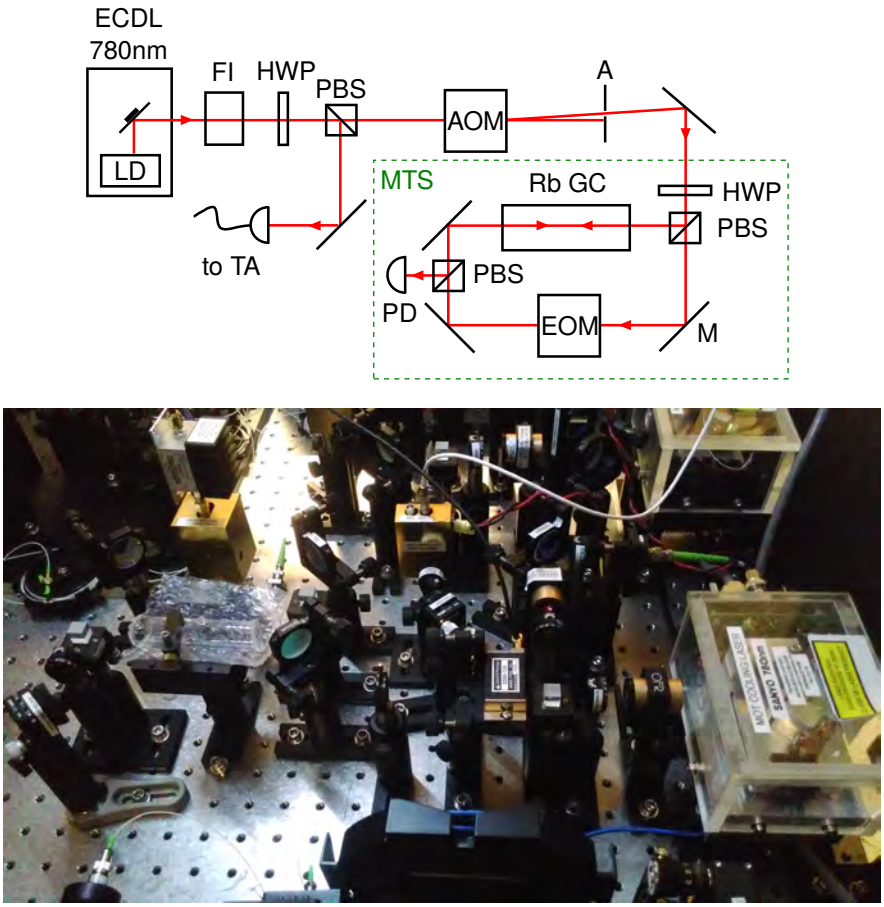

Figure 2.8: (Top) The schematic of the cooling laser module. (Bottom) The picture of the module.

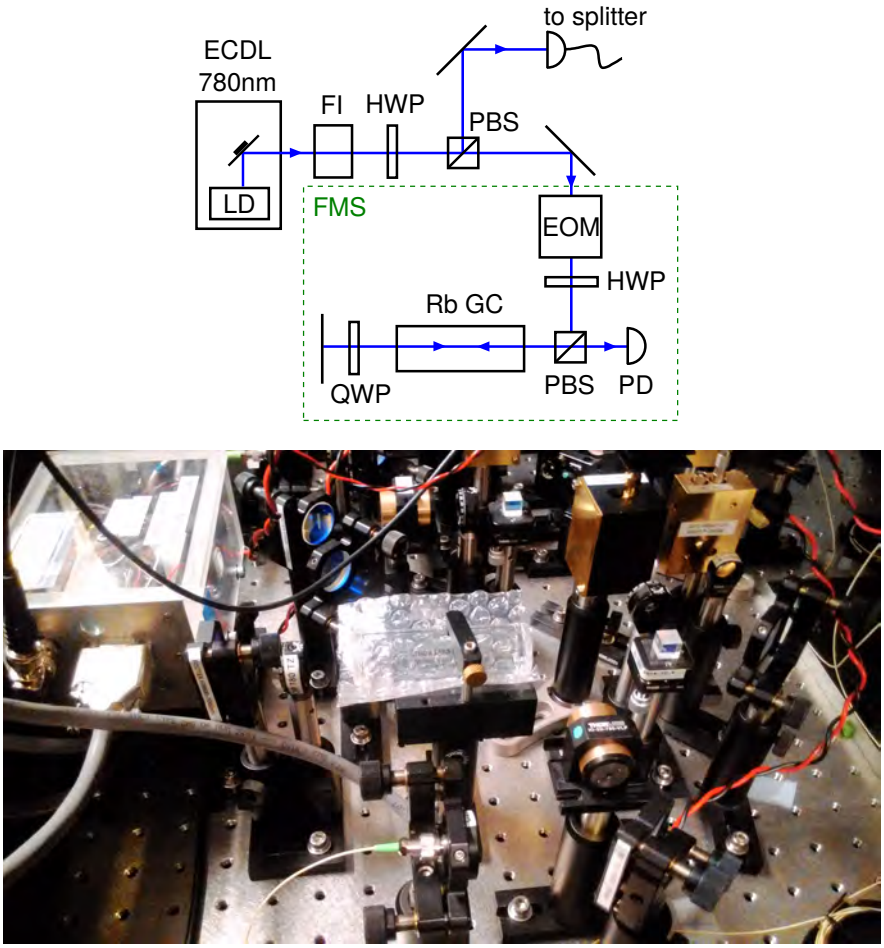

Figure 2.9: (Top) The schematic of the repump laser module. (Bottom) The picture of the module.

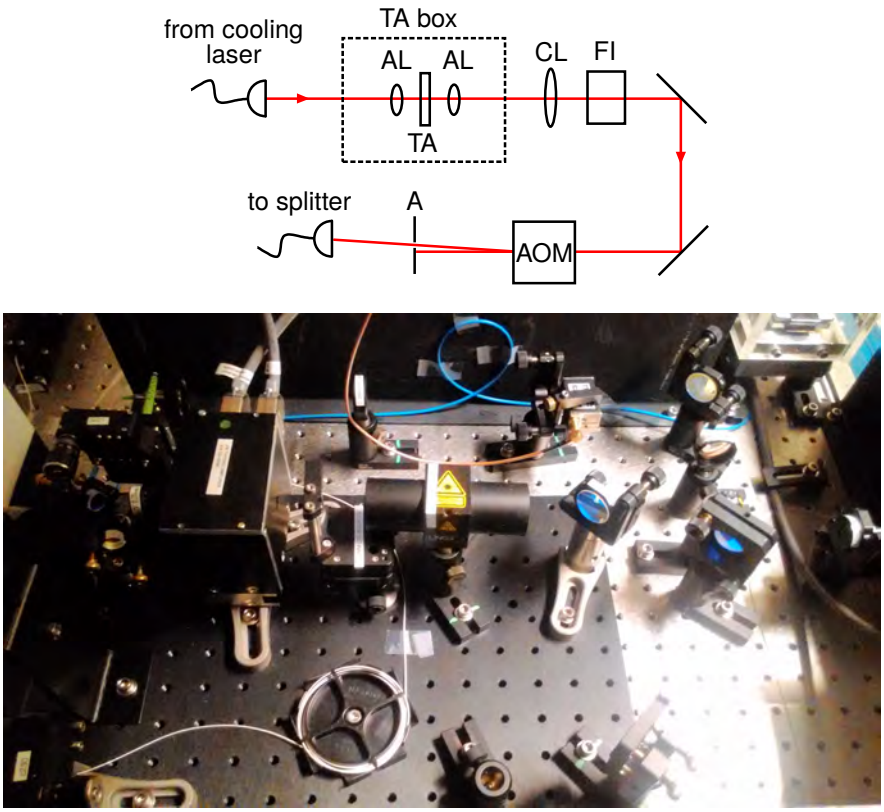

Figure 2.10: (Top) The schematic of the tapered amplifier module. (Bottom) The picture of the module.

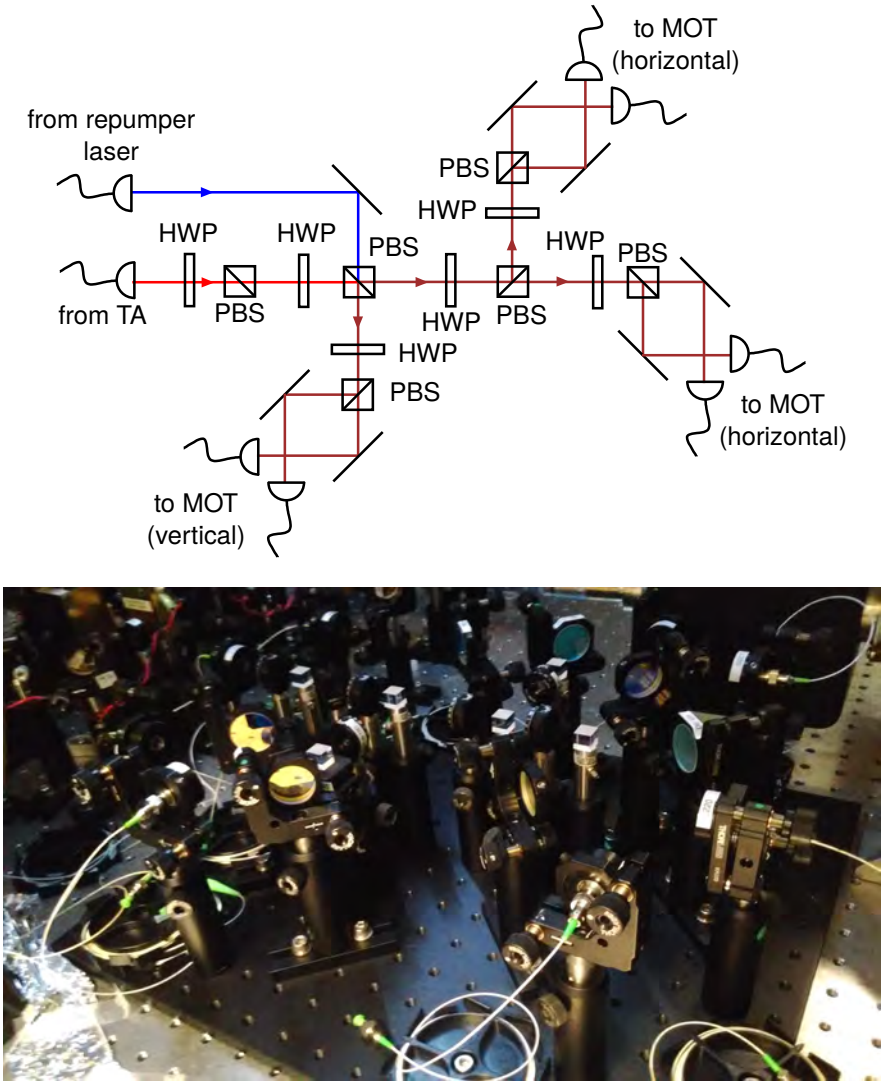

Figure 2.11: (Top) The schematic of the splitter module. (Bottom) The picture of the module.

using a home-built peltier controller. The incoming seed laser beam is coupled to the TA chip with an aspheric lens (AL), while the outgoing amplified beam is 'collimated' with another AL. As the outgoing 'collimated' beam still has different beam divergences on different axes due to the tapering effect, we used another cylindrical lens (CL) to correct for the effect and maximize the coupling efficiency.

The schematic of the TA module is depicted in Figure 2.10. Light from the cooling laser module is coupled into the TA chip, which amplifies it from around 15 mW to around 1 W. The outgoing amplified light is then passed through a 60dB optical isolator (FI) to prevent any feedback which might damage the TA chip. From FI, the beam passes through an AOM, and is then coupled into a fibre.

Splitter Module

The schematic of the splitter module is depicted in Figure 2.11. The amplified cooling light and the repump light are combined in the splitter module, and split into 6 beams with equal cooling light power; the proportion of the repump light in each beam should not matter. The amplified cooling light initially passes through a PBS to 'clean' the polarisation. This ensures that the splitting ratios do not change even if the polarisation of the incoming cooling light changes.

In principle, we can create beams with unbalanced cooling light power by rotating the appropriate HWPs. We might explore this option in the future if necessary.

MOT Optics

The schematic of the MOT optics is depicted in Figure 2.12. We expect the size of the cloud to be a few millimetres. For the cooling laser intensity to be roughly constant

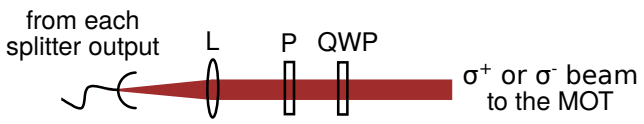

Figure 2.12: A few optical components just before the MOT to create large and circularly polarised beams.

throughout the cloud, we require a large cooling volume of the MOT. Thus, we expand each of the six beams by using a lens (f = 100 mm) to be around 1 inch in diameter. Just before the MOT, we clean the polarisation once more using a linear polariser, and then we use a QWP to create either σ^+ or σ^- beams.

2.3 Vacuum System

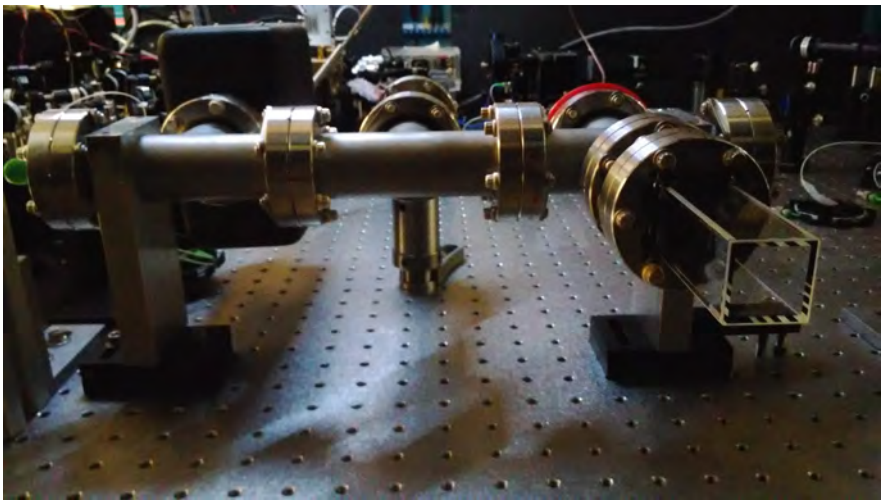

Figure 2.13: The picture of the vacuum system.

The last ingredient that we need for a MOT is an ultrahigh vacuum (UHV) system with pressure of around 10^{-9} mbar. To do so, we assembled the vacuum chamber, and installed a cuvette (a glass cell designed to provide an easy optical access to inside the vacuum chamber), a pinch-off tube, an ion pump (Varian StarCell), an ion gauge, and a Rb dispenser. A picture of the vacuum system is depicted in Figure 2.13.

Initially, we pumped the air out of the chamber using a turbomolecular pump via the pinch-off tube. We monitored the vacuum pressure using a pirani gauge, which was installed alongside the pump. In the process of pumping, we checked for possible leakages. After the chamber reached a sufficiently low pressure (around 10^{-6} mbar), we performed a bake-out of the vacuum chamber by heating it up to accelerate the degasification process of the remaining 'junk' material inside the chamber. This process

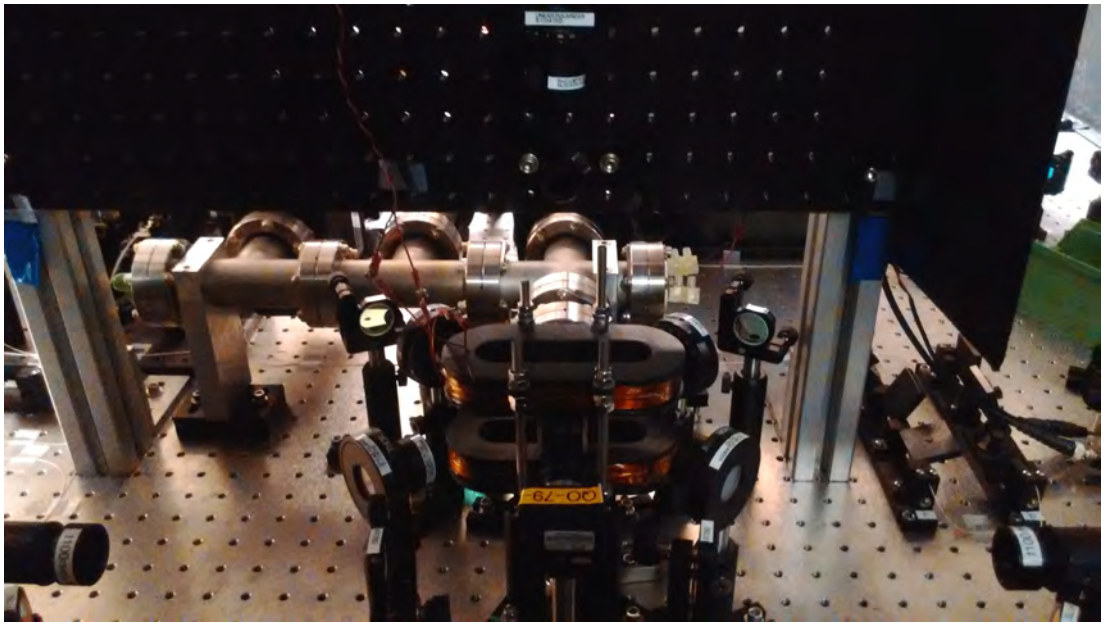

Figure 2.14: The picture of the experimental setting: inside the cuvette we expect a cold elongated cloud of ^{87}Rb.

took a few days. After the pressure stabilised at around 10^{-8} mbar, we sealed the pinch-off tube, and removed the turbomolecular pump and the pirani gauge.

Then, we switched on the ion pump, which brought the chamber to even lower pressure by creating strong electric and magnetic field to ionize and capture the remaining gas inside the chamber. We used the ion gauge to monitor the pressure inside the chamber, and we managed to reach a pressure of around 10^{-9} mbar, which is good enough for our experiments. We can then create a vapour of Rb atoms in the vacuum chamber by passing a current through the Rb dispenser.

After the vacuum system was ready, we positioned the racetrack coils around the cuvette, and installed the MOT optics. We also placed an infrared camera to observe fluorescence from the Rb atoms. A picture of the experimental setting is shown in Figure 2.14.

Chapter 3

Conclusion and Outlook

We started this thesis by proposing that an elongated cloud of cold atoms might be a solution to generate a brighter source of narrowband photon pairs, and we have described in detail the process of designing and constructing the various necessary components to obtain the cloud: magnetic field, laser system and vacuum system. Now, we conclude this thesis with a picture of elongated cloud of cold ^{87}Rb atoms and a short discussion on the outlook of this project.

3.1 A Sight of The Cloud

The picture of the elongated cloud is shown in Figure 3.1. From the picture, we estimate the size of the cloud to be around 3.2 mm in the elongation axis and 1.3 mm in the other axis, resulting in elongated ratio of around 2.5.

We played with the cloud and noticed a few things. Firstly, the overall size of the cloud depends on the coil current; the larger the current, the smaller the cloud size. This is because larger coil current produces larger magnetic field gradient, resulting in higher trapping force. Secondly, we can slightly vary the shape of the cloud by intentionally misaligning or creating an imbalance in some of the beams. This gives us some flexibility in varying the size and shape of the cloud to the geometry that we desire.

Figure 3.1: The picture of the elongated cloud of cold ^{87}Rb. For this cloud, we set the red detuning of the cooling laser as 10 MHz. The coil current was around 2.5 A, while the power on each MOT beams (around 1 inch in diameter) is around 20 mW.

From the picture, we see that there appears to be blobs on the cloud around 0.5 mm in size. We are still in the process of investigating why the blobs exist. We highly suspect that it is due to some wierd wrinkly pattern (with periodicity of around 0.5 mm) in the linear polarizers (Thorlabs LPNIRE100-B). We will try other linear polarizers or use one inch PBS cubes in the future.

3.2 Outlook

As we have already obtained the elongated cloud, the next logical step is to characterise the optical density in different axes with different cloud geometry. Then, we will

proceed towards narrowband photon pair generation using four-wave mixing cascade decay scheme, and explore the effect of cloud geometry and optical density on the bandwidth and brightness of the generated photons. We hope that we can obtain a brighter source of narrowband photon pairs, which will be a very valuable resource to further our exploration in the photon-atom interation.

Appendix A

Working Principles of Magneto-optical Trap

Magneto-optical trap (MOT) has been used extensively in the cooling and trapping of neutral atoms. It exploits the Zeeman and hyperfine structure of the atoms to apply position and velocity dependent radiation pressure to cool and trap the atoms. It was first demonstrated with sodium atoms by Raab et. al. [35]. An excellent overview of the atomic dynamics inside a MOT is given in [36].

The MOT setup is relatively easy to build and maintain, as it does not require high magnetic field and the trap is still robust even though the beams are unbalanced. We can also easily supply Rb atoms to the MOT using a commercial getter Rb source [37].

Here we briefly explain the working principle of the MOT. There are three basic ingredients necessary to trap and cool neutral atoms inside a MOT: a good vacuum, quadrupole magnetic field (usually produced by anti-Helmholtz circular coils), and three pairs of counter propagating and circularly polarized beams (red-detuned to a cycling transition) in 3 different directions. We might also need some repump lasers to bring the atoms back to the cycling transition, if there is a possibility of the atoms decaying to dark hyperfine levels.

The mechanism for MOT cooling and trapping in one direction is described in

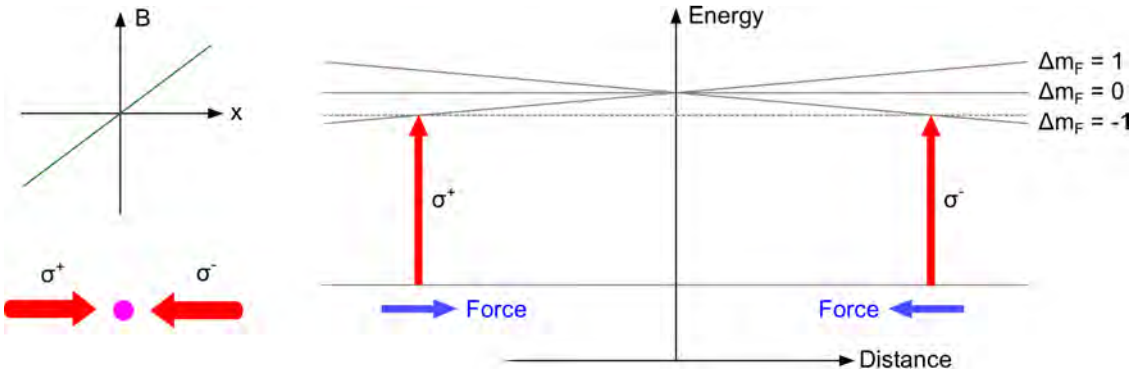

Figure A.1: The working principle of MOT in one dimension. (Left, top) Quadrupole magnetic field results in a constant magnetic field gradient near the centre of the trap. (Left, bottom) The ensemble is subjected to counter propagating, circularly polarized beams. (Right) The red detuned laser interact stronger with a certain Zeeman hyperfine level, resulting in a radiative force towards the centre of the trap.

Figure A.1; this can be easily extended to three dimensions. Note that we require the laser beams in 3 different directions, although they do not necessarily be perpendicular to each other. This allows for more flexibility in the design of the MOT.

The atoms in the MOT undergo cooling process due to the Doppler effect. As the laser beams are red detuned from the resonance, the moving atoms absorb more photons in the opposite direction compared to photons in the same direction (due to the Doppler shift). The emitted photons, however, do not have any preferred direction. Thus, there is a net momentum transfer from the photons to the atoms which decreases the atomic velocity and cools down the atoms.

To illustrate the trapping process in the MOT, refer to Figure A.1. Anti-Helmholtz coils produce nearly constant magnetic field gradients in the vicinity of the trap centre, with the trap centre itself having zero magnetic field. This results in Zeeman energy splitting for atomic states with different magnetic quantum numbers (m_F). Consider a transition from F to $F+1$ state. The possible transitions are the ones at which $\Delta m_F = 0, \pm 1$, where $\Delta m_F = m_{F+1} - m_F$. If an atom is displaced rightwards from the centre of the trap, the red-detuned laser is closer to resonance with the σ^- transitions

($\Delta m_F = -1$) than the σ^+ transitions ($\Delta m_F = 1$) . Thus, in average, the atoms undergo more σ^- transitions, while the scattered photons radiates isotropically. Due to the radiation pressure of the σ^- laser beam, the atoms experience a force leftwards to the centre to the trap. The reverse is also true for leftwards displaced atoms. Hence, the clever placement of the laser beams and magnetic field results in a cooling process and restoring force towards the centre of the trap, enabling cooling and trapping of neutral atoms.

A. WORKING PRINCIPLES OF MAGNETO-OPTICAL TRAP

Appendix B

Laser Spectroscopy

We present here a brief overview of the two laser spectroscopy techniques that we use: frequency modulation spectroscopy (FMS) and modulation transfer spectroscopy (MTS). We obtain from laser spectroscopy the error signal, which depicts how far off is the current laser frequency from the atomic transition frequency. The error signal can then be used to lock and stabilise our laser to a specific atomic transition by using a feedback control loop. Using these spectroscopy techniques, we can obtain narrowband lasers in the order of 1 MHz bandwidth. This laser stabilisation technique is very similar to Pound-Drever-Hall (PDH) frequency locking technique [38], with the atoms replacing the role of the cavity. A comprehensive review on laser spectroscopy can be found in [39].

B.1 Frequency Modulation Spectroscopy

The scheme of frequency modulation spectroscopy [1] (FMS) is depicted in Figure B.1. The laser beam from the ECDL is modulated by an EOM, producing two sidebands at $\omega - \Delta$ and $\omega + \Delta$, where ω is the laser frequency and Δ is the modulation frequency. The modulated beam passes through the gas cell (as a pump beam), and is then reflected and passes through the same path again (as a probe beam). The counter propagating

[1] A more complete name is Doppler-free saturated-absorption frequency modulation spectroscopy, but for simplicity we just call it frequency modulation spectroscopy.

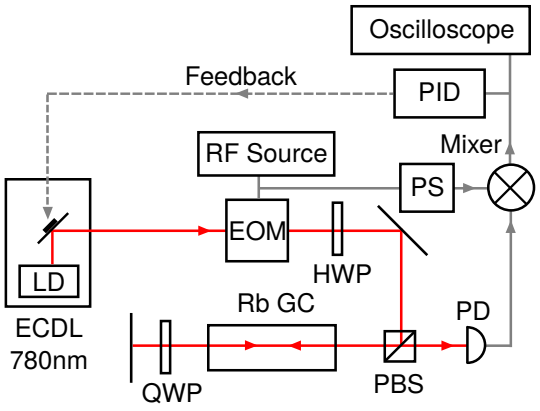

Figure B.1: The scheme of frequency modulation spectroscopy. The radio frequency (RF) source providing the modulation signal to the EOM is a home-built direct digital synthesizer (DDS).

pump and probe beam inside the gas cell (in the saturated absorption regime) allows us to address only atoms of zero-velocity class, and hence suppressing Doppler broadening effect [40]. The probe beam is detected by a photodiode (PD). The signal from the PD is then mixed with the modulation signal, which produces the error signal. The phase shifter (PS) creates a phase shift between the signals before the mixing process, allowing us some variations of the error signal. A thorough description of FMS can be found in [41].

In order to lock our lasers, we first supply a sawtooth or triangle signal (scanning signal) to the piezo in the ECDL. This will scan the laser frequency over a small range. Near the atomic transition, we can see on oscilloscope the error signal, which serves as a fingerprint of a specific transition. The error signal of the $5^2S_{1/2}$ (F = 2) to $5^2P_{3/2}$ transitions in ^{87}Rb atoms (at $\Delta = 23$ MHz) is shown in Figure B.3. Note that at this point the laser is still scanning and not yet locked to a specific transition. Now, we vary the voltage offset in the piezo such that, if the scanning signal is switched off, the laser frequency is very close the targeted transition. We then switch off the scanning signal and switch on the proportional-integral-derivative (PID) controller. This PID controller will feedback on the piezo and stabilise the laser over any fluctuations.

FMS suffers from large background error signal, which is due to effect of modulation

in the off-resonant regime. This background error signal depends strongly on the laser intensity. If the laser intensity fluctuates, the variation in the background error signal might cause the locking point to shift, and this affect the stability and bandwidth of the locked laser.

B.2 Modulation Transfer Spectroscopy

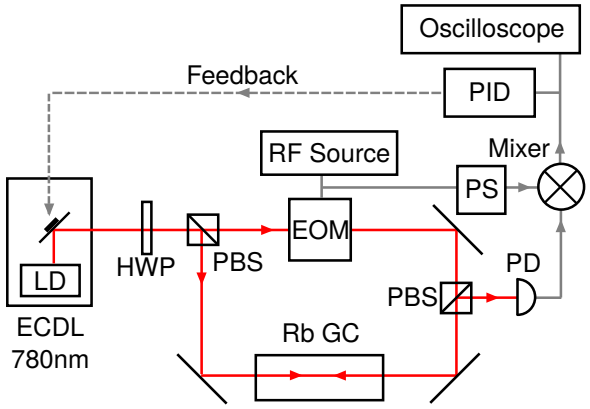

Figure B.2: The scheme of modulation transfer spectroscopy, which is very similar to the FMS, but with slight modifications.

The modulation transfer spectroscopy (MTS) technique is depicted in Figure B.2. It was first demonstrated in Rb atoms by McCarron et. al. [42]. The difference between MTS and FMS is that only the pump beam is modulated in MTS. The modulation from the pump beam can be 'transfered' via a four wave mixing process to the probe beam only in the near resonance region ($\sim$ transition linewidth). Thus, MTS removes the problem of having a large background error signal, and this allows for effective laser stabilisation even with fluctuations in the laser intensity. The comparison of the oscilloscope trace between FMS and MTS is given in Figure B.3.

However, only cycling transitions produce strong error signals. In Figure B.3, the strongest error signal comes from the F = 2 to F' = 3 transition (although we can probably still lock the laser to the F = 2 to F' = (2,3) crossover). We need frequency shifter such as AOM in order to lock the laser to a non-cycling transition.

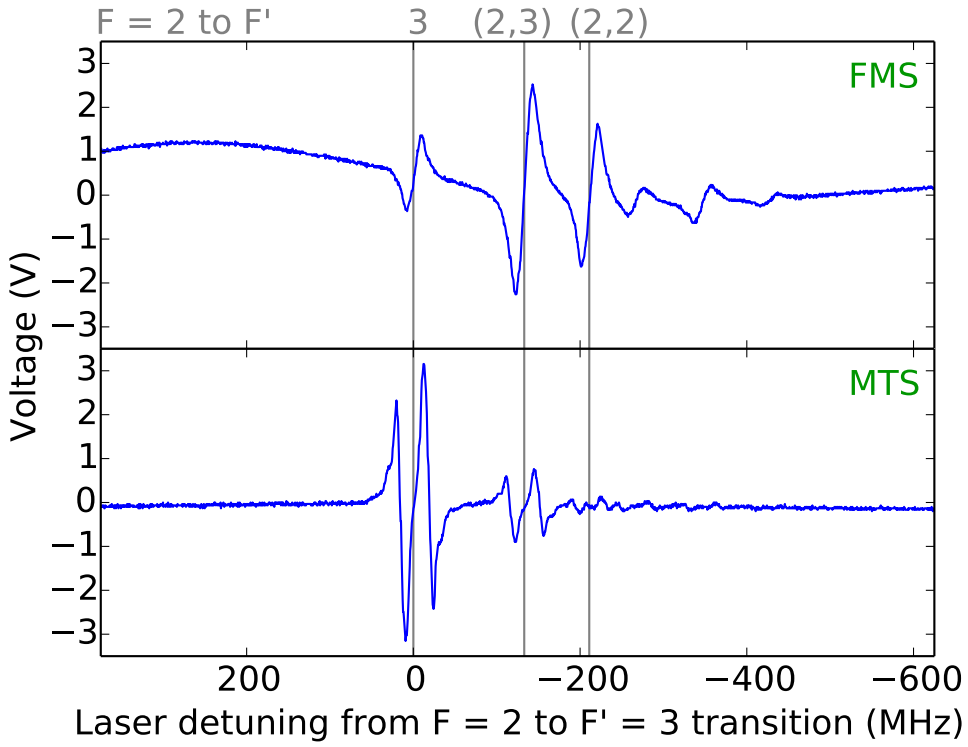

Figure B.3: The comparison of the oscilloscope trace of the error signals produced with FMS and MTS (in the region of $5^2S_{1/2}$ (F = 2) to $5^2P_{3/2}$ transitions of ^{87}Rb atoms). The modulation frequency of EOM is $\Delta = 23$ MHz.

References

[1] P. Shor. **Algorithms for quantum computation: discrete logarithms and factoring**. *Proceedings 35th Annual Symposium on Foundations of Computer Science*, pages 124–134, 1994.

[2] J. M. Raimond, M. Brune, and S. Haroche. **Colloquium: Manipulating quantum entanglement with atoms and photons in a cavity**. *Reviews of Modern Physics*, **73**(3):565–582, 2001.

[3] H. Häffner, C. Roos, and R. Blatt. **Quantum computing with trapped ions**. *Physics Reports*, **469**(4):155–203, 2008.

[4] H. J. Briegel, T. Calarco, D. Jaksch, J. I. Cirac, and P. Zoller. **Quantum computing with neutral atoms**. *Journal of Modern Optics*, **47**(2-3):415–451, 2000.

[5] L. M. K. Vandersypen and I. L. Chuang. **NMR techniques for quantum control and computation**, 2004.

[6] J. R. Petta, A. C. Johnson, J. M. Taylor, E. A. Laird, A. Yacoby, M. D. Lukin, C. M. Marcus, M. P. Hanson, and A. C. Gossard. **Coherent manipulation of coupled electron spins in semiconductor quantum dots**. *Science*, **309**(5744):2180–2184, 2005.

[7] M. H. Devoret and R. J. Schoelkopf. **Superconducting circuits for quantum information: an outlook.** *Science (New York, N.Y.)*, **339**(6124):1169–74, 2013.

[8] K.-A. Suominen. **44 - Physical Implementation of Large-Scale Quantum Computation**. In *Handbook of Natural Computing*, pages 1493–1520. 2012.

[9] D. P. DiVincenzo. **The Physical Implementation of Quantum Computation**. *Fortschritte der Physik*, **48**(9-11):771–783, 2000.

[10] B. Srivathsan, G. K. Gulati, B. Chng, G. Maslennikov, D. Matsukevich, and C. Kurtsiefer. **Narrow band source of transform-limited photon pairs via four-wave mixing in a cold atomic ensemble**. *Physical Review Letters*, **111**(12):123602, 2013.

REFERENCES

[11] M. K. Tey, Z. Chen, S. A. Aljunid, B. Chng, F. Huber, G. Maslennikov, and C. Kurtsiefer. **Strong interaction between light and a single trapped atom without the need for a cavity**. *Nature Physics*, **4**(12):924–927, oct 2008.

[12] M. Sondermann and G. Leuchs. **Photon-Atom Coupling with Parabolic Mirrors**. In *Engineering the Atom-Photon Interaction*, pages 75–98. 2015.

[13] V. Leong, M. A. Seidler, M. Steiner, A. Cerè, and C. Kurtsiefer. **Time-Resolved Scattering of a Single Photon by a Single Atom**. Unpublished Manuscript, 2016.

[14] Y. Wang, J. Miná, L. Sheridan, and V. Scarani. **Efficient excitation of a two-level atom by a single photon in a propagating mode**. *Physical Review A*, **83**(6):063842, 2011.

[15] B. Srivathsan. *Heralded Single Photons for Efficient Interaction With Single Atoms*. PhD thesis, National University of Singapore, 2014.

[16] G. K. Gulati. *Narrowband Photon Pairs From a Cold Atomic Vapour for Interfacing With a Single Atom*. PhD thesis, National University of Singapore, 2015.

[17] S. Friberg, C. Hong, and L. Mandel. **Measurement of time delays in the parametric production of photon pairs.** *Physical review letters*, **54**(18):2011–2013, may 1985.

[18] W. Tittel, J. Brendel, H. Zbinden, and N. Gisin. **Violation of Bell Inequalities by Photons More Than 10 km Apart**. *Physical Review Letters*, **81**(17):3563–3566, oct 1998.

[19] T. Chanelière, D. N. Matsukevich, S. D. Jenkins, T. A. B. Kennedy, M. S. Chapman, and A. Kuzmich. **Quantum telecommunication based on atomic cascade transitions**. *Physical Review Letters*, **96**(9), 2006.

[20] C. Kurtsiefer, M. Oberparleiter, and H. Weinfurter. **High-efficiency entangled photon pair collection in type-II parametric fluorescence**. *Physical Review A*, **64**(2):023802, jul 2001.

[21] M. D. Reid and D. F. Walls. **Violations of classical inequalities in quantum optics**. *Physical Review A*, **34**(2):1260–1276, aug 1986.

[22] S. Du, P. Kolchin, C. Belthangady, G. Y. Yin, and S. E. Harris. **Subnatural linewidth biphotons with controllable temporal length**. *Physical review letters*, **100**(18):183603, may 2008.

[23] G. K. Gulati, B. Srivathsan, B. Chng, A. Cerè, D. Matsukevich, and C. Kurtsiefer. **Generation of an exponentially rising single-photon field from parametric conversion in atoms**. *Physical Review A - Atomic, Molecular, and Optical Physics*, **90**(3):033819, 2014.

[24] B. Srivathsan, G. K. Gulati, A. Cerè, B. Chng, and C. Kurtsiefer. **Reversing the temporal envelope of a heralded single photon using a cavity**. *Physical Review Letters*, **113**(16):163601, 2014.

[25] D. A. Steck. **Rubidium 87 D Line Data**. *Journal of Geophysical Research*, **2009**(2):31, 2010.

[26] R. H. Dicke. **Coherence in spontaneous radiation processes**. *Physical Review*, **93**(1):99–110, 1954.

[27] M. Gross and S. Haroche. **Superradiance: An essay on the theory of collective spontaneous emission**. *Physics Reports*, **93**(5):301–396, dec 1982.

[28] H. Jen. **Superradiant cascade emissions in an atomic ensemble via four-wave mixing**. *Annals of Physics*, **360**:556–570, sep 2015.

[29] J. Schoser, A. Batär, R. Löw, V. Schweikhard, A. Grabowski, Y. B. Ovchinnikov, and T. Pfau. **Intense source of cold Rb atoms from a pure two-dimensional magneto-optical trap**. *Physical Review A*, **66**(2):023410, aug 2002.

[30] K. Dieckmann, R. Spreeuw, M. Weidemüller, and J. Walraven. **Two-dimensional magneto-optical trap as a source of slow atoms**. *Physical Review A*, **58**(5):3891–3895, 1998.

[31] S. Zhang, C. Liu, S. Zhou, C. S. Chuu, M. M. T. Loy, and S. Du. **Coherent control of single-photon absorption and reemission in a two-level atomic ensemble**. *Physical Review Letters*, **109**(26):263601, 2012.

[32] E. Jones, T. Oliphant, and P. Peterson. **SciPy: Open Source Scientific Tools for Python**, 2001.

[33] J. D. Hunter. **Matplotlib: A 2D Graphics Environment**. *Computing in Science & Engineering*, **9**:90–95, 2007.

[34] A. S. Arnold, J. S. Wilson, and M. G. Boshier. **A simple extended-cavity diode laser**. *Review of Scientific Instruments*, **69**(3):1236, mar 1998.

[35] E. Raab, M. Prentiss, A. Cable, S. Chu, and D. Pritchard. **Trapping of neutral sodium atoms with radiation pressure.** *Physical review letters*, **59**(23):2631–2634, dec 1987.

REFERENCES

[36] C. G. Townsend, N. H. Edwards, C. J. Cooper, K. P. Zetie, C. J. Foot, A. M. Steane, P. Szriftgiser, H. Perrin, and J. Dalibard. **Phase-space density in the magneto-optical trap**. *Physical Review A*, **52**(2):1423–1440, aug 1995.

[37] U. D. Rapol, A. Wasan, and V. Natarajan. **Loading of a Rb magneto-optic trap from a getter source**. *Physical Review A*, **64**(2):023402, jun 2001.

[38] E. D. Black. **An introduction to PoundDreverHall laser frequency stabilization**. *American Journal of Physics*, **69**(1):79, jan 2001.

[39] W. Demtröder. *Laser Spectroscopy: Basic Concepts And Instrumentation*. Springer Science & Business Media, 2013.

[40] T. W. Hänsch, S. A. Lee, R. Wallenstein, and C. Wieman. **Doppler-Free Two-Photon Spectroscopy of Hydrogen 1 S 2 S**. *Physical Review Letters*, **34**(6):307–309, feb 1975.

[41] J. M. Supplee, E. A. Whittaker, and W. Lenth. **Theoretical description of frequency modulation and wavelength modulation spectroscopy.** *Applied optics*, **33**(27):6294–302, sep 1994.

[42] D. J. McCarron, S. A. King, and S. L. Cornish. **Modulation transfer spectroscopy in atomic rubidium**. *Measurement Science and Technology*, **19**(10):105601, 2008.